analytical chemistry

pubs.acs.org/ac Article

Electrochemical Biosensors Capable of Detecting Biomarkers in Human Serum with Unique Long-Term Antifouling Abilities Based on Designed Multifunctional Peptides

Guixiang Wang,[‖] Rui Han,[‖] Qun Li, Yinfeng Han, and Xiliang Luo*

Cite This: *Anal. Chem.* 2020, 92, 7186−7193 Read Online

ACCESS | Metrics & More | Article Recommendations | Supporting Information

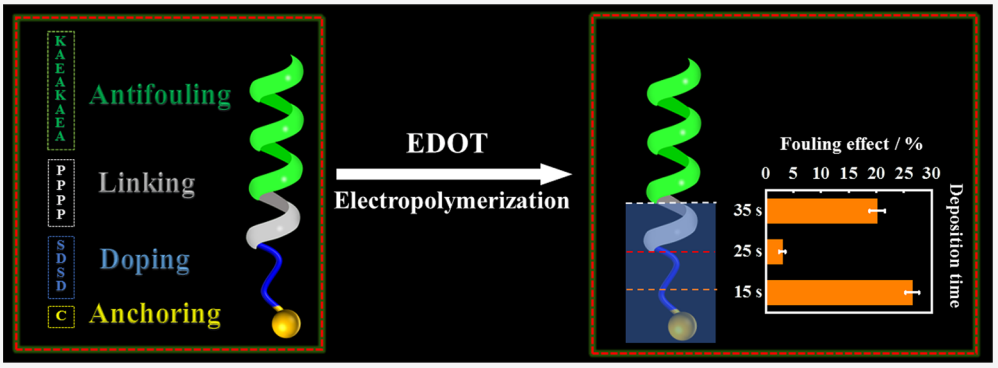

ABSTRACT: An electrochemical sensing platform for biomarker detection in complex serum samples with unique long-term antifouling performance was constructed, based on newly designed multifunctional peptides containing anchoring, doping, linking, and antifouling sequences. The designed peptides were first attached onto an electrode surface with the assistance of the anchoring sequences, and the negatively charged doping sequences as dopants for conducting polymer poly(3,4-ethylenedioxythiophene) (PEDOT) were then precisely doped into the electropolymerized PEDOT to form a conducting and stable substrate, leaving the linking and antifouling sequences exposed on the PEDOT substrate surface. The linking sequence of the peptide between the doping and antifouling parts was designed to be beneficial for enhancing the antifouling performance. After the biorecognizing probe immobilization, the obtained biosensor was able to detect targets with a low limit of detection of 2.3 fM and high specificity in complex biological fluids. More importantly, the electrochemical biosensor exhibited incomparable long-term antifouling performances over previous reports and retained their antifouling capabilities for 20 days, indicating a promising feasibility of this design strategy for the construction of biosensors and bioelectronics to be used or implanted in real biological systems.

The rapid, accurate, and specific detection of disease markers directly in serum has promising application to clinical diagnosis.[1,2] Among the current assaying methods, electrochemical biosensors have attracted increasing attention due to their high sensitivity, specificity, and low cost.[3,4] The main challenge for biosensors to be used in complex biological media is the severe nonspecific adsorption or fouling on the sensing interfaces, which makes them passivated or even lose selection performance.[5] Great efforts have been devoted to resolve this difficult problem. 6-Mercaptohexanol (MCH)[6] or bovine serum albumin (BSA)[7] was often introduced to biosensor interfaces as a blocking regent, respectively, to resist the fouling effect. Unfortunately, MCH cannot resist fouling in human blood serum, which is rich in various proteins, although it has a certain antifouling capability to decrease single protein adsorption.[8] BSA has certain antifouling properties in serum, but it will reduce the sensitivity of biosensors.[2]

Recently, poly(ethylene glycol) (PEG) and zwitterionic materials are widely used in the fabrication of antifouling biosensors.[2,9] PEG, the "gold standard" of antifouling polymers, has many mature commercial derivatives, which are broadly used in sensors and electronics.[4,10,11] However, poor antioxidation ability limits their long-term application.[12] More importantly, in many cases, they cannot present excellent antifouling performance in human blood serum. Zwitterionic materials (such as carboxybetaine, phosphorylcholine, and sulfobetaine) have been considered as promising antifouling materials for the next generation.[13−15] They exhibited excellent

Received: February 19, 2020
Accepted: April 14, 2020
Published: April 14, 2020

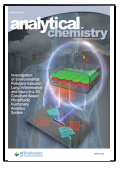

https://dx.doi.org/10.1021/acs.analchem.0c00738
Anal. Chem. 2020, 92, 7186−7193

antifouling abilities because they can form hydration shells via ionic solvation.[16,17] But the synthesis of methacrylate derivative monomers (such as carboxybetaine methacrylate and sulfobetaine methacrylate) used for biosensor preparation is complex, and their commercialized products are generally not available. Moreover, the reaction conditions of such monomer polymerization are demanding. Therefore, these defects and deficiencies of the above antifouling materials limit their application in the construction of low fouling biosensors.

Peptides, which are commonly used in medicine and biotechnology,[18−20] have attracted much attention due to their unique properties (their structures contain amino and carboxyl groups) similar to zwitterionic materials.[21−24] Furthermore, due to their advantages of flexible function and shape, easy modification and preparation, and environmental friendliness, peptides can be designed flexibly according to requirements.[18,25,26] A series of antifouling biosensors based on zwitterionic peptides have been reported. The sequence of CPPPPEKEKEKE, possessing negatively charged glutamic acid (E) and positively charged lysine (K),[27] has been demonstrated to be resistant to cell adhesion,[28] human serum,[8] and even whole blood adsorption.[3] The zwitterionic CRERERE peptide sequence has shown good antifouling behaviors, and the nonspecific adsorption of 1.0 mg mL^{-1} single-protein solutions (BSA, lysozyme, and β-lactoglobulin) on its self-assembled monolayers was below 5.0 ng cm^{-2} (the commonly accepted ultralow fouling criterion).[29] Recently, our group has successively designed different peptides with the sequences of (EESKSESKSGGGGC),[30] CPPPPQNQNQNQ,[31] and (CPPPPEK2-(EK)4(EK)) (branched zwitterionic peptide),[32] which exhibited excellent antifouling performances and were successfully applied in low fouling biosensors. However, most of these antifouling biosensors were not investigated for long-term applications, and the continuous antifouling capabilities of peptides[32] or sensing interfaces[3,8,26,30,33] in complex media were unknown. Only very few reports about antifouling biosensors have investigated the long-term antifouling performances, and it turned out that the antifouling capabilities were significantly impaired just within a few hours when the biosensors were continuously soaked in complex biological media-like serum.[31] Therefore, it is critical to develop biosensors with satisfying long-term antifouling properties, so as to meet the requirements for practical applications, especially for implantable sensors or biosensors.

Additionally, peptides are of poor conductivity,[3,8] which greatly limits their application in electrochemical sensors and biosensors, especially for *in vivo* detection. The conducting polymer poly(3,4-ethylenedioxothiophene) (PEDOT), which is widely investigated because of its unique conductivity, stability, and biocompatibility, has a wide range of applications in the construction of biosensors and bioelectronics.[34−36] It is very popular to prepare nanocomposites with excellent properties by doping PEDOT with electronegative dopants.[11,37] In view of this, we have designed a novel multifunctional peptide with a sequence of CDSDSPPPPAEAKAEAK gathering the anchoring, doping, linking, and antifouling segments, using one cysteine (C) as the anchor to self-assemble the peptide onto the surface of gold nanoparticles (AuNPs) electrodeposited on a polished glassy carbon electrode (GCE) via a Au−S bond. The doping sequence (DSDS) charged negatively was used as the dopant for PEDOT electrochemical polymerization, and it can be exactly doped into the PEDOT to form a conducting thin film, significantly enhancing the stability and conductivity of the substrate and enabling the antifouling sequence (AEAKAEAK) to be exposed on the surface of the PEDOT film. The linking sequence (PPPP) that connected the doping and the antifouling sequences is favorable to assist the antifouling sequence to form a dense antifouling layer.[28] In this work, microRNA 21 (miRNA-21), commonly used as a biomarker for disease diagnosis and therapy,[38] was selected as a typical target, and its aptamer was further immobilized on the antifouling peptide to fabricate an antifouling electrochemical biosensor, which was capable of assaying miRNA-21 in the serum of breast cancer patients.

EXPERIMENTAL SECTION

Reagents. The multifunctional peptide (CDSDSPPPPAEAKAEAK) and the reference peptide (CPPPPAEAKAEAK) were synthesized (purity >95%) by Bankpeptide Biological Technology Co., Ltd. (Hefei, China), and the chromatogram and the mass spectra data of multifunctional peptides are shown in Figure S1 of the Supporting Information. The lysozyme (Lys), myoglobin (Mb), BSA, fluorescein isothiocyanate-labeled BSA (FITC-BSA), and fluorescein diacetate (FDA) for the surface nonspecific adsorption experiments were all purchased from Adamas-beta Reagent (Shanghai, China). The hydrogen tetrachloroauric (III) acid ($HAuCl_4{\cdot}3H_2O$) and 3,4-ethylenedioxythiophene (EDOT) monomer were purchased from Aladdin Chemistry Co., Ltd. (Shanghai, China). The miRNA-21, miRNA-21 aptamer, miRNA-141, let-7a, and miRNA-122 were synthesized by Sangon Co., Ltd. (Shanghai, China), and the detailed sequences are shown in Table S1. DEPC-treated ultrapure water (Sangon, Shanghai, China) was used for dilution of all miRNA solution and patient serum samples. Dulbecco's modified Eagle's medium (DMEM) was purchased from Sigma Co., Ltd. (Aldrich, St. Louis, MO, USA). Serum samples from healthy humans and patients with breast cancer were provided by the Eighth People's Hospital of Qingdao (Qingdao, China), and the informed consent for use of the human serum was obtained. All the sample preparations were authorized by the institutional review board of the Eighth People's Hospital of Qingdao and were performed in compliance with the institutional guidelines and relevant laws. Other reagents were analytical reagents and used without further purification. The water with a resistivity greater than 18 MΩ cm was used throughout the experiment and purified using a Milli-Q system (Millipore Co., Bedford, MA, USA). Excluding the supplementary description, the default peptides used in the experiment were multifunctional peptides.

Apparatus. All electrochemical measurements and experiments were performed with a CHI 660E electrochemical workstation (Shanghai CH Instrument Co., China) at room temperature. A three-electrode system composed of a bare or modified GCE as the working electrode, a saturated calomel electrode (SCE) as the reference electrode, and a platinum wire as the auxiliary electrode, was used throughout. Cyclic voltammetry (CV) and amperometric *i-t* curve techniques were used for electrodeposition of AuNPs and PEDOT, respectively. Biosensor measurements were recorded in phosphate buffer saline (PBS, 10.0 mM, pH 7.4) containing 5.0 mM $[Fe(CN)_6]^{3-/4-}$ and 0.1 M KCl by differential pulse voltammetry (DPV), with the potential range from −0.2 to 0.6 V at an amplitude of 50 mV, a pulse period of 0.5 s, and a potential increment of 4.0 mV.

https://dx.doi.org/10.1021/acs.analchem.0c00738
Anal. Chem. 2020, 92, 7186−7193

Scheme 1. Schematic Description of Preparation of Electrochemical miRNA-21 Biosensor Based on Conducting Polymer PEDOT and Designed Multifunctional Peptide

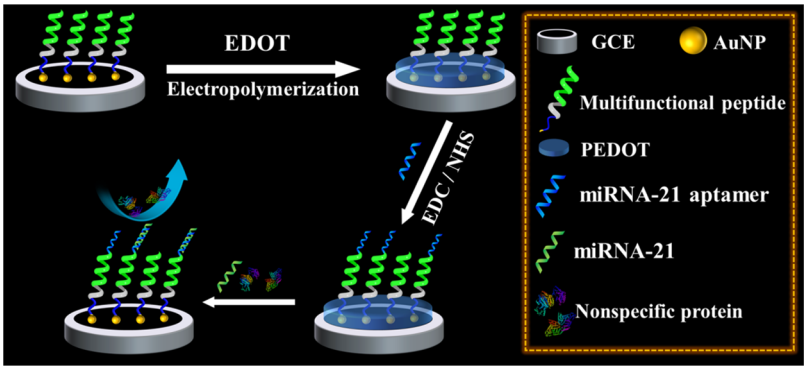

X-ray photoelectron spectroscopy (XPS) was performed using a Thermo ESCALAB 250Xi spectrometer microprobe (Thermo-VG Fisher Scientific, USA) with a monochromatic Al Kα X-ray source ($h\nu = 15$ kV), and all spectra were standardized by the value of the C 1s peak (284.6 eV). Protein adsorption testing was performed by using a TCS-SP5 confocal microscope (Leica, Germany). The hydrophilic properties of different modified surfaces were measured by the static water contact angles using a JC2000D1 system (Shanghai Zhongchen, China). The charges of peptides were determined by measuring the zeta potential using a Nano-ZS Zetasizer ZEN3600 (Malvern, Ltd., UK). Circular dichroism (CD) spectra were recorded on a JASCO J-810 spectropolarimeter (Jasco Inc., Japan). In addition, a Vortex 3 shaker (IKA, Germany) and MST-80 thermostatic incubator (Taitan, China) were also employed to ensure homogenization of the solutions and suitable incubation temperature.

Characterization of Designed Peptides. The charges of the multifunctional peptide and reference peptide were characterized by the zeta potential. The secondary structure information of the peptide was examined using CD spectra in the wavelength range of 190−270 nm with a step width of 0.2 nm, with subtracted buffer spectra from the peptide sample spectra. The water contact angle was also measured to examine the hydrophilicity of the surfaces with or without peptides.

Preparation of Antifouling Interface. The fabrication procedure of the antifouling interface is illustrated in Scheme 1. GCE was successively polished with 1.0, 0.3, and 0.05 μm Al_2O_3 slurry and ultrasonically washed with absolute alcohol and Millipore water for 2 min, respectively. Afterward, the GCE was immersed in 4 mL of 0.5 mmol L^{-1} $HAuCl_4$ aqueous solution containing 0.5 M KNO_3 and scanned from −1.5 to 0.5 V at the scanning rate of 50 mV s^{-1} to electrochemically deposit AuNPs on the GCE surface (AuNP/GCE). Multifunctional peptides were self-assembled onto the surface of AuNPs by soaking the AuNP/GCE in 0.14 mM peptide aqueous solution for 12 h at room temperature, and the Pep/AuNP/GCE was obtained after a thorough rinsing with Millipore water. Subsequently, 7.4 mM EDOT monomers were dissolved thoroughly in 5 mL of water by ultrasonication and then electropolymerized onto the surface of the Pep/AuNP/GCE via an amperometric *i-t* curve technique at a potential of 1.0 V for 25 s. As a result, the PEDOT/Pep/AuNP/GCE with an antifouling interface was prepared.

Immobilization of miRNA-21 Aptamer. Here, 10.0 μL of 2.0 μM miRNA-21 aptamers modified with carboxyl groups was added to 10.0 μL of 0.4 M EDC and 0.1 M NHS in PBS (10.0 mM, pH 7.0) with continuous stirring for 30 min, and then, the PEDOT/Pep/AuNP/GCE with antifouling peptides on its surface was incubated in the above mixed solution for 2 h at 37 °C. After thorough rinsing with Millipore water, a stable biosensor (Apt/PEDOT/Pep/AuNP/GCE) was obtained.

Characterization of Antifouling Performance. Confocal laser scanning microscopy with an excitation wavelength of 488 nm was used to test the protein absorption and cell adhesion capability of the modified surfaces. Electrodes modified with AuNPs but without peptides were used as controls. The modified electrodes were incubated in 1.0 mg mL^{-1} FITC-BSA solution for 24 h at 37 °C and thoroughly rinsed with Millipore water, and then, the fluorescence images of these electrode surfaces were characterized by confocal laser scanning microscopy.

Similarly, for the cell adhesion test, three electrodes were placed in an A549 cell (human lung cancer cells) culture medium (cell density of 1×10^5 cells mL^{-1}) and incubated in the humidified cell incubator at 37 °C with 5% CO_2 for 24 h, respectively. Next, 0.10 mg mL^{-1} fresh FDA was prepared and used to stain the active A549 cells in the dark for 5 min under aerobic conditions and washed with Dulbecco's phosphate buffered saline (DPBS, Gibco). Finally, fluorescent images were captured to monitor the adhesion of A549 cells on electrode surfaces after FDA entering the living cells.

Detection of miRNA-21. The biosensor was incubated in different concentrations of miRNA-21 in PBS (10.0 mM, pH 7.4) for 45 min at 37 °C, and the changes of electrochemical signals before and after specific binding with miRNA-21 were measured by DPV within the range from −0.2 to 0.6 V in PBS (10.0 mM, pH 7.4) containing 5.0 mM $[Fe(CN)_6]^{3-/4-}$ and 0.1 M KCl. The biosensor was applied to assay targets in 10% (V/V) serum of three breast cancer patients. The recovery experiments were carried out to further verify the potential application of the biosensor in real blood samples.

RESULTS AND DISCUSSION

Investigation of Designed Multifunctional Peptides. It has been reported that hydrophobic interaction and charge attraction are the key factors for the interface fouling.[16,39,40] Therefore, the design of antifouling materials with hydrophilic and electro-neutral properties may meet the requirements of antifouling performance. The isoelectric point (PI) of the designed multifunctional peptide (CDSDSPPPPAEAKAEAK) is 3.97, and the zeta potential is measured as −38.1 mV (Figure

https://dx.doi.org/10.1021/acs.analchem.0c00738
Anal. Chem. 2020, 92, 7186−7193

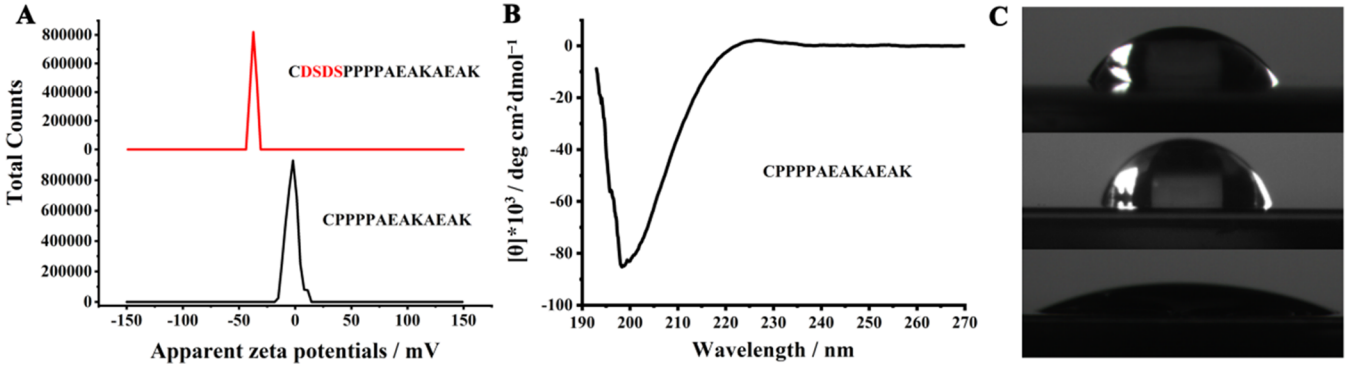

Figure 1. (A) Zeta potential of the multifunctional peptide and reference peptide. (B) CD spectra of 0.3 mg mL^{-1} reference peptide in PBS (10.0 mM, pH 7.4). (C) Contact angle images corresponding to GCE, AuNP/GCE, and Reference Pep/AuNP/GCE (from top to bottom), respectively.

1A), which is negatively charged because of the presence of the doping sequence (−DSDS−). Once the doping sequence is electropolymerized with the conducting polymer PEDOT, the antifouling sequence (PPPPAEAKAEAK) will be exposed on the PEDOT surface. In order to investigate its antifouling performance, the reference peptide (CPPPPAEAKAEAK) was also designed and used for characterization. The PI of the reference peptide is 7.05, and its zeta potential is very close to 0.0 mV (Figure 1A), indicating that the excellent electrical neutrality and potential antifouling property that can avoid nonspecific adsorption through charge attraction.

The secondary structure of the reference peptide was assessed by CD spectroscopy. As shown in Figure 1B, a strong negative absorption band near 205 nm and a weaker positive absorption band near 225 nm were observed, indicating a typical extended polyproline (P)-generated helix conformation. This result suggested that the reference sequence is favorable for the peptide to form an organized and dense antifouling layer on the surface to strengthen its antifouling performance.[28,31]

To verify the hydrophilicity of the antifouling sequence, the static water contact angle was measured on different surfaces. As shown in Figure 1C, the contact angle of AuNP/GCE is 75.83 ± 1.47°, which is larger than that of the bare GCE (54.69 ± 1.54°), indicating a hydrophobic property of the surface. However, after the reference peptide was self-assembled on AuNP/GCE, the water contact angle significantly reduced to 22.94 ± 1.25°, which is consistent with the excellent hydrophilicity of other reported peptide layers,[3,32] showing promising potential antifouling capability.

Construction of Electrochemical Antifouling Biosensor. To confirm the successful modification steps, XPS was used to characterize the change of the characteristic elements content on different modified surfaces. On the surface of Pep/AuNP/GCE, there are two strong photoelectron signals of AuNPs corresponding to Au $4f_{7/2}$ (84 eV) and Au $4f_{5/2}$ (88 eV),[3,41] respectively (Figure S2A, inset). The signal of S 2p (162 eV) confirmed that the multifunctional peptide was successfully self-assembled on the AuNP/GCE surface (Figure S2A). After the electrodeposition of PEDOT, the signal of N 2s (409 eV) significantly declined, and the signal of the S element slightly increased (Figure S2B). The signal peak of P 2p (135 eV) appeared after the immobilization of the miRNA-21 aptamer (a single-strand DNA with phosphate skeleton) (Figure S2C).[4,33] Hence, the element content changes of each modification step verified the successful deposition or attachment of AuNPs, peptide, PEDOT, and aptamer.

To further confirm the successful construction of the biosensor, DPV was further carried out to characterize each modification step. After AuNPs electrodeposition on the GCE, the oxidation current signal of the $[Fe(CN)_6]^{3-/4-}$ probe (Figure 2, curve b) became larger than that of the bare GCE

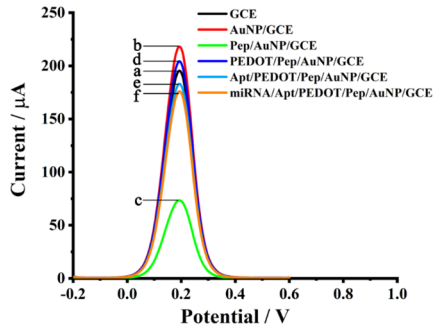

Figure 2. DPV responses of different modified electrodes in PBS (10.0 mM pH 7.4) containing 5.0 mM $[Fe(CN)_6]^{3-/4-}$ and 0.1 M KCl:(a) bare GCE, (b) AuNP/GCE, (c) Pep/AuNP/GCE, (d) PEDOT/Pep/AuNP/GCE, (e) Apt/PEDOT/Pep/AuNP/GCE, and (f) miRNA-21/Apt/PEDOT/Pep/AuNP/GCE.

(Figure 2, curve a), due to the fact that AuNPs greatly increase the surface area of the electrode and promote electron transfer.[3] The current signal declined significantly after the self-assembly of the multifunctional peptide onto the AuNP/GCE (Figure 2, curve c), owing to the poor conductivity and electronegativity of the peptide, which impeded and repulsed electron transfer of the probe. However, a remarkably increased current signal was observed after PEDOT electrodeposition (Figure 2, curve d), as the substrate composed of PEDOT and a doping peptide possessed excellent conductivity. Subsequently, the current signal decreased again followed the immobilization of the miRNA-21 aptamer (Figure 2, curve e) and the specific binding of the miRNA-21 target (Figure 2, curve f), because the aptamer and miRNA-21 with negatively charged phosphate skeletons repel the electron transfer of electroactive probes to the electrode surface. Therefore, distinct current signal changes of each step indicate the successful construction of the biosensor, and the signal changes associated with the specific binding of targets can be used for the detection of miRNA-21.

Effects of PEDOT Deposition Time on Antifouling and Sensing Performances. As long as the doping sequences of multifunctional peptides are exactly and

https://dx.doi.org/10.1021/acs.analchem.0c00738
Anal. Chem. 2020, 92, 7186−7193

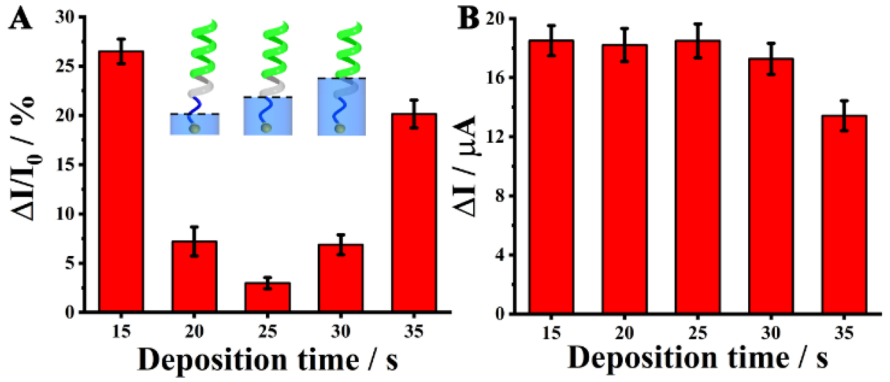

Figure 3. Effects of PEDOT deposition time on the antifouling performance of the biosensor in 25% (V/V) healthy human serum (A) and sensing response of the biosensor to 10.0 pM miRNA-21 (B). The schematic diagrams in panel (A) correspond to the PEDOT deposition times of 15, 25, and 30 s, respectively, from left to right. Error bars represent the standard deviations of three repeated determinations.

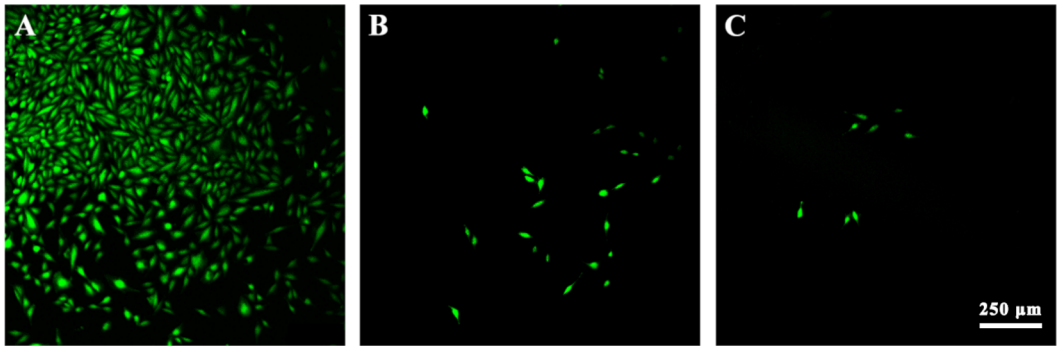

Figure 4. Fluorescence images of cells attached on (A) AuNP-, (B) Pep/AuNP-, and (C) PEDOT/Pep/AuNP-modified surfaces. All the modified surfaces were incubated in A549 cells for 24 h at 37 °C.

completely doped within the electrodeposited PEDOT, the best antifouling and sensing performance of the biosensor will be obtained. That is, the performance of the biosensor, especially the antifouling capability, greatly depends on the deposition time of PEDOT, as it will control the thickness of the deposited PEDOT film. Therefore, the effects of different times of PEDOT deposition on the antifouling and sensing performance of the biosensor were explored in detail, as shown in Figure 3. When the deposition time was shorter than 25 s, part of the negatively charged doping sequences might not be covered by the PEDOT, and those doping sequences exposed on the surface will allow protein adsorption due to electrostatic interactions, leading to poor antifouling performance of the biosensor. When the PEDOT deposition time was longer than 25 s, the antifouling property was not good either. In this case, on one hand, part of the antifouling sequences of the multifunctional peptides may be covered by the deposited PEDOT, weakening the antifouling capability of the sensing interface. On the other hand, the proline sequences may also be covered by the PEDOT, which will reduce the helix conformation formed by the proline sequence, resulting in a less compact arrangement of the antifouling sequences and thus impair the ability of antifouling.[28] While at the PEDOT deposition time of 25 s, the doping sequences were entirely covered by the PEDOT but kept the linking proline sequences and antifouling sequences exposed on the surface, corresponding to the best antifouling performance of the biosensor. Similarly, as shown in Figure 3B, an ideal sensing signal was also obtained for the biosensor at the deposition time of 25 s.

Investigation of Antifouling Performance. To evaluate the antifouling property of the PEDOT/Pep/AuNP surface, cell attachment experiments were carried out using A549 cells. The surfaces modified with AuNP, Pep/AuNP, and PEDOT/Pep/AuNP were incubated in A549 cells (1×10^5 cells mL^{-1}) for 24 h. As shown in Figure 4A, the fluorescent image of the AuNP-modified surface exhibited serious cell adhesion. However, after self-assembly of a multifunctional peptide, the fluorescence intensity observably decreased (Figure 4B), suggesting that the designed antifouling peptide was able to prevent the adhesion of cells. Fortunately, the antifouling performance of the surface was further strengthened after the electrodeposition of PEDOT (Figure 4C), and few cells were attached to the PEDOT/Pep/AuNP surface. As PEDOT totally neutralized the negative charges of the doping sequence of the multifunctional peptide, leaving the antifouling sequence exposed on the surface of PEDOT to resist cell adhesion. The results of the FITC-BSA adsorption tests on the PEDOT/Pep/AuNP surface (Figure S3) are consistent with those of the cell adhesion studies, further confirming the excellent antifouling property of the multifunctional peptide.

Additionally, the antifouling properties of different electrode surfaces were explored using three single proteins, BSA, Mb, and Lys, which are negative, neutral, and positive in charge, respectively. The lower the change rate of the electrochemical current signal is, the better the antifouling performance of the electrode surface is. As shown in Figure S4, a clear current change was observed on the MCH/AuNP/GCE (MCH was used here as a reference for comparison) after incubation in single protein solutions for 30 min, while there was only a very

https://dx.doi.org/10.1021/acs.analchem.0c00738
Anal. Chem. 2020, 92, 7186−7193

tiny signal change on the PEDOT/Pep/AuNP/GCE, indicating outstanding antifouling performance. A similar antifouling performance of electrode surfaces can also be seen in experiments with a series of various concentrations of human sera. As shown in Figure 5, the current change rate of the PEDOT/Pep/AuNP/GCE was only 2.86% in undiluted human serum (100%, V/V). Even more importantly, after the miRNA-21 aptamer immobilization, the signal change rate of the Apt/PEDOT/Pep/AuNP/GCE remained very low, which only changed by 1.74% and 2.50% after soaking in 10% and 25% (V/V) human sera, respectively. Relevant DPV curves are shown in Figure S5. These results demonstrate an excellent antifouling performance of the PEDOT surface functionalized with the newly designed antifouling peptide sequence, even after further immobilization of certain biorecognition elements as biosensing probes.

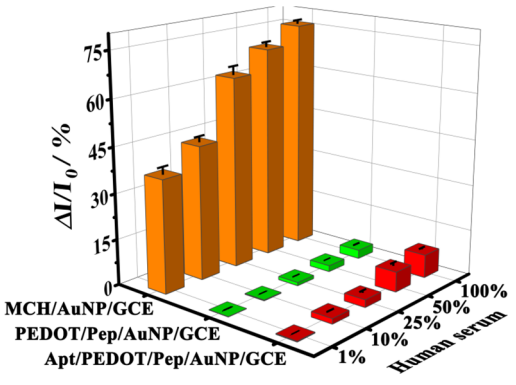

Figure 5. Current signal change rates of MCH/AuNP/GCE, PEDOT/Pep/AuNP/GCE, and Apt/PEDOT/Pep/AuNP/GCE in a series of healthy human sera. The current signal change rate is represented as $(\Delta I/I_0)\%$, $\Delta I = I_0 - I$, where I_0 and I refer to the current signal value before and after incubation of protein. Error bars represent the standard deviations of three repeated determinations.

The long-term antifouling property is a critical factor for sensors,[42] especially those applied for *in vivo* detection.[43] An assessment of the long-term antifouling performances of different surfaces in human serum is shown in Figure 6. After soaking in 25% (V/V) human serum for 8 h, the current signal change rate of the MCH/AuNP/GCE was as high as 70.84%, while those of the surfaces modified with PEDOT and multifunctional peptides (PEDOT/Pep/AuNP/GCE and Apt/PEDOT/Pep/AuNP/GCE) only changed by 2.85% and 4.53%, respectively. This long-term antifouling result is significantly superior to those of most of the antifouling biosensors reported in the literatures.[31,44] After soaking in serum for 20 days, the signal of the MCH/AuNP/GCE unexpectedly changed by about 93.14%, while those of the PEDOT/Pep/AuNP/GCE and Apt/PEDOT/Pep/AuNP/GCE only varied by 9.08% and 14.93%, respectively. These results demonstrate that the PEDOT surface functionalized with the peptides has superior stability and long-term antifouling capability.

Detection of Target miRNA-21. To achieve the best sensing performance of the biosensor, the incubation time for miRNA-21 to bind with its specific aptamer was studied. As shown in Figure S6, when the incubation time was 45 min, the specific binding reached the equilibrium. Under the optimal experimental conditions, an assessment of the biosensor response to miRNA-21 with concentrations from 10.0 fM to 1.0 nM was performed (Figure S7). The linear regression equation is $\Delta I = -69.55 \lg (C) - 4.70$, with a correlation coefficient (R^2) of 0.9962 in the concentration range from 10.0 fM to 0.1 nM. The limit of detection (LOD) was estimated as 2.3 fM (S/N = 3), which is lower than or comparable to those of most previous reports[45−52] (Table S2). Such a low LOD of the biosensor may be ascribed to the advantages of the doping peptide−PEDOT substrate (with excellent stability, biocompatibility, and conductivity) and the antifouling peptide (that is tightly packed and exhibits outstanding antifouling property), which provided a low noise signal for higher specific recognition of miRNA-21.

Specificity and Reproducibility of Biosensor. The selectivity of the biosensor was evaluated by monitoring its exposure to different RNAs in the serum, such as miRNA-141, miRNA-122, miRNA-223, let-7a, one and three mismatched miRNA-21, and the mixture (Mix) of all these RNAs (Figure S8). Even at concentrations 100 times the concentration of miRNA-21, the signal responses of other RNAs are all significantly lower than that of the specific target miRNA-21, showing excellent specificity of the biosensor.

Reproducibility is a crucial criterion for the evaluation of biosensors, and the intra-assay and interassay reproducibilities of the developed biosensor were investigated with 1.0 pM miRNA-21. The relative standard deviations (RSD) of the intrabatch (Figure S9A) and interbatch (Figure S9B) are 0.54% and 1.27%, respectively ($n = 5$), which showed excellent reproducibility of the biosensor based on the PEDOT and multifunctional peptide.

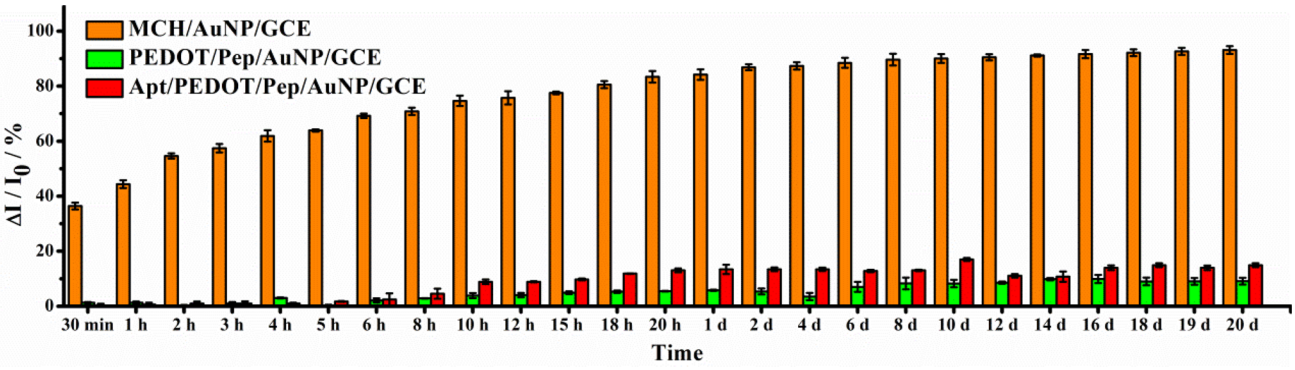

Figure 6. Long-term antifouling performance of MCH/AuNP/GCE, PEDOT/Pep/AuNP/GCE, and Apt/PEDOT/Pep/AuNP/GCE in 25% (V/V) healthy human serum for an extended period. Error bars represent the standard deviations of three repeated determinations.

https://dx.doi.org/10.1021/acs.analchem.0c00738
Anal. Chem. 2020, 92, 7186−7193

Table 1. Analytical Results for miRNA-21 Detection in 10% (V/V) Serum Samples from Breast Cancer Patients

Sample[a]	Measured (pM)	Added (pM)	Found (pM)	Recovery (%)	RSD (%, n = 3)
Sample 1	0.023 ± 0.0026	1	0.98 ± 0.017	95.80	1.73
Sample 1	0.023 ± 0.0026	10	10.64 ± 0.66	106.16	6.20
Sample 1	0.023 ± 0.0026	60	59.36 ± 3.59	98.80	6.05
Sample 2	0.072 ± 0.0023	1	1.09 ± 0.052	101.68	4.77
Sample 2	0.072 ± 0.0023	10	9.97 ± 0.43	98.99	4.31
Sample 2	0.072 ± 0.0023	60	61.03 ± 2.68	101.59	4.39
Sample 3	0.22 ± 0.032	1	1.19 ± 0.07	97.54	5.88
Sample 3	0.22 ± 0.032	10	10.27 ± 0.39	100.49	3.80
Sample 3	0.22 ± 0.032	60	59.36 ± 1.44	98.57	2.43

[a]Samples 1−3 refer to serum samples from three patients with breast cancer.

Clinical Serum Sample Analysis. To assess the potential clinical application of the antifouling biosensor, serum samples from three patients with breast cancer were first tested, and the recovery experiments were further carried out with miRNA-21 in 10% (V/V) human serum (Table 1). The miRNA-21 concentration in serum samples was obtained by direct detection with the biosensor, and the recoveries for miRNA-21 were measured and ranged from 95.80% to 106.16%. These results indicate the promising potential of the biosensor for auxiliary clinical detection of cancer biomarkers based on the newly designed antifouling peptide.

CONCLUSIONS

A novel and universal antifouling electrochemical sensing platform based on the conducting polymer PEDOT and designed peptides was developed. The multifunctional peptides and electrodeposited PEDOT can form a stable and conductive substrate, leaving the antifouling sequence of the multifunctional peptide exposed on the PEDOT surface. Compared with conventional antifouling materials, the prepared PEDOT surface functionalized with an antifouling peptide displayed excellent antifouling performance, outstanding electrical conductivity, and long-term antifouling capability. Low fouling and highly sensitive electrochemical biosensors were easily prepared through biorecognition probe immobilization on the antifouling peptide, and the constructed biosensors were capable of assaying targets in complex biological media conveniently. In short, the inspired design of an antifouling strategy based on PEDOT and multifunctional peptides provided a promising way to construct other biosensors and bioelectronics operating in complex media, especially for the development of implantable devices considering the unique long-term antifouling capability.

ASSOCIATED CONTENT

Supporting Information

The Supporting Information is available free of charge at https://pubs.acs.org/doi/10.1021/acs.analchem.0c00738.

Information on multifunctional peptides; detailed sequences of DNA and RNA; XPS characterization; antifouling characterization; incubation time of miRNA-21; sensing, selectivity, and reproducibility of the biosensor (PDF)

AUTHOR INFORMATION

Corresponding Author

Xiliang Luo − *Key Laboratory of Optic-electric Sensing and Analytical Chemistry for Life Science, MOE, Shandong Key Laboratory of Biochemical Analysis, College of Chemistry and Molecular Engineering, Qingdao University of Science and Technology, Qingdao 266042, China;* orcid.org/0000-0001-6075-7089; Phone: + 86 532 84022860; Email: xiliangluo@qust.edu.cn; Fax: + 86 532 84023681

Authors

Guixiang Wang − *Key Laboratory of Optic-electric Sensing and Analytical Chemistry for Life Science, MOE, Shandong Key Laboratory of Biochemical Analysis, College of Chemistry and Molecular Engineering, Qingdao University of Science and Technology, Qingdao 266042, China; College of Chemistry and Chemical Engineering, Taishan University, Taian 271021, China*

Rui Han − *Key Laboratory of Optic-electric Sensing and Analytical Chemistry for Life Science, MOE, Shandong Key Laboratory of Biochemical Analysis, College of Chemistry and Molecular Engineering, Qingdao University of Science and Technology, Qingdao 266042, China*

Qun Li − *College of Chemistry and Chemical Engineering, Taishan University, Taian 271021, China*

Yinfeng Han − *College of Chemistry and Chemical Engineering, Taishan University, Taian 271021, China*

Complete contact information is available at: https://pubs.acs.org/10.1021/acs.analchem.0c00738

Author Contributions

‖G. Wang and R. Han contributed equally to this work.

Notes

The authors declare no competing financial interest.

ACKNOWLEDGMENTS

The work is supported by the National Natural Science Foundation of China (21675093, 21974075, and 51702228), the Shandong Provincial Natural Science Foundation (ZR2019MB039 and ZR2017BEM014), the Taishan Scholar Program of Shandong Province of China (ts20110829), the Shandong Key Laboratory of Biochemical Analysis (SKLBA1905), and the Doctoral Found of Taishan University (Y-01-2018018 and 2019HX099).

REFERENCES

(1) Wu, L.; Qu, X. G. *Chem. Soc. Rev.* **2015**, *44*, 2963−2997.
(2) Vaisocherová, H.; Brynda, E.; Homola, J. *Anal. Bioanal. Chem.* **2015**, *407*, 3927−3953.
(3) Wang, G.; Su, X.; Xu, Q.; Xu, G.; Lin, J.; Luo, X. *Biosens. Bioelectron.* **2018**, *101*, 129−134.
(4) Hui, N.; Sun, X.; Niu, S.; Luo, X. *ACS Appl. Mater. Interfaces* **2017**, *9*, 2914−2923.

(5) Gooding, J. J. *Nat. Nanotechnol.* **2019**, *14*, 1089−1090.
(6) Xiang, J.; Pi, X.; Chen, X.; Xiang, L.; Yang, M.; Ren, H.; Shen, X.; Qi, N.; Deng, C. *Biosens. Bioelectron.* **2017**, *96*, 268−274.
(7) Tian, C.; Wang, L.; Luan, F.; Fu, X.; Zhuang, X.; Chen, L. *Chem. Commun.* **2019**, *55*, 12479−12482.
(8) Cui, M.; Wang, Y.; Wang, H.; Wu, Y.; Luo, X. *Sens. Actuators, B* **2017**, *244*, 742−749.
(9) Lowe, S.; O'Brien-Simpson, N. M.; Connal, L. A. *Polym. Chem.* **2015**, *6*, 198−212.
(10) Wang, G.; Xu, Q.; Liu, L.; Su, X.; Lin, J.; Xu, G.; Luo, X. *ACS Appl. Mater. Interfaces* **2017**, *9*, 31153−31160.
(11) Cui, M.; Song, Z.; Wu, Y.; Guo, B.; Fan, X.; Luo, X. *Biosens. Bioelectron.* **2016**, *79*, 736−741.
(12) Zhang, X.; Brodus, D.; Hollimon, V.; Hu, H. *Chem. Cent. J.* **2017**, *11*, 1−12.
(13) Jiang, S.; Cao, Z. *Adv. Mater.* **2010**, *22*, 920−932.
(14) He, M.; Gao, K.; Zhou, L.; Jiao, Z.; Wu, M.; Cao, J.; You, X.; Cai, Z.; Su, Y.; Jiang, Z. *Acta Biomater.* **2016**, *40*, 142−152.
(15) Xiong, Z. J.; Shen, M. W.; Shi, X. Y. *Bioconjugate Chem.* **2019**, *30*, 2519−2527.
(16) Liu, B.; Liu, X.; Shi, S.; Huang, R.; Su, R.; Qi, W.; He, Z. *Acta Biomater.* **2016**, *40*, 100−118.
(17) Leng, C.; Sun, S.; Zhang, K.; Jiang, S.; Chen, Z. *Acta Biomater.* **2016**, *40*, 6−15.
(18) Tao, K.; Makam, P.; Aizen, R.; Gazit, E. *Science* **2017**, *358*, eaam9756.
(19) Sun, H.; Hong, Y. X.; Xi, Y. J.; Zou, Y. J.; Gao, J. Y.; Du, J. Z. *Biomacromolecules* **2018**, *19*, 1701−1720.
(20) Zhao, J.; Chen, H.; Tang, Y.; Chen, H.; Chen, G.; Yin, Y.; Li, G. *J. Mater. Chem. B* **2018**, *6*, 2510−2523.
(21) Xu, C.; Hu, X.; Wang, J.; Zhang, Y.-M.; Liu, X.-J.; Xie, B.-B.; Yao, C.; Li, Y.; Li, X.-S. *ACS Appl. Mater. Interfaces* **2015**, *7*, 17337−17345.
(22) Cheung, D. L.; Lau, K. H. A. *Langmuir* **2019**, *35*, 1483−1494.
(23) Sakala, G. P.; Reches, M. *Adv. Mater. Interfaces* **2018**, *5*, 1800073.
(24) Gaw, S. L.; Sakala, G.; Nir, S.; Saha, A.; Xu, Z. J.; Lee, P. S.; Reches, M. *Biomacromolecules* **2018**, *19*, 3620−3627.
(25) Li, H.; Li, W.; Liu, F.; Wang, Z.; Li, G.; Karamanos, Y. *Anal. Chem.* **2016**, *88*, 3662−3668.
(26) Ding, C.; Wang, X.; Luo, X. *Anal. Chem.* **2019**, *91*, 15846−15852.
(27) Chen, S.; Cao, Z.; Jiang, S. *Biomaterials* **2009**, *30*, 5892−5896.
(28) Nowinski, A. K.; Sun, F.; White, A. D.; Keefe, A. J.; Jiang, S. *J. Am. Chem. Soc.* **2012**, *134*, 6000−6005.
(29) Ye, H.; Wang, L.; Huang, R.; Su, R.; Liu, B.; Qi, W.; He, Z. *ACS Appl. Mater. Interfaces* **2015**, *7*, 22448−22457.
(30) Cui, M.; Wang, Y.; Jiao, M. X.; Jayachandran, S.; Wu, Y. M.; Fan, X. J.; Luo, X. L. *ACS Sens.* **2017**, *2*, 490−494.
(31) Liu, N.; Hui, N.; Davis, J. J.; Luo, X. *ACS Sens.* **2018**, *3*, 1210−1216.
(32) Liu, N. Z.; Song, J. Y.; Lu, Y. W.; Davis, J. J.; Gao, F. X.; Luo, X. L. *Anal. Chem.* **2019**, *91*, 8334−8340.
(33) Wang, G.; Han, R.; Su, X.; Li, Y.; Xu, G.; Luo, X. *Biosens. Bioelectron.* **2017**, *92*, 396−401.
(34) Liu, X.; Xiao, T.; Wu, F.; Shen, M.-Y.; Zhang, M.; Yu, H.-h.; Mao, L. *Angew. Chem., Int. Ed.* **2017**, *56*, 11802−11806.
(35) Wu, H.; Lee, C.-J.; Wang, H.; Hu, Y.; Young, M.; Han, Y.; Xu, F.-J.; Cong, H.; Cheng, G. *Chem. Sci.* **2018**, *9*, 2540−2546.
(36) Wu, J. G.; Chen, J. H.; Liu, K. T.; Luo, S. C. *ACS Appl. Mater. Interfaces* **2019**, *11*, 21294−21307.
(37) Wang, G.; Morrin, A.; Li, M.; Liu, N.; Luo, X. *J. Mater. Chem. B* **2018**, *6*, 4173−4190.
(38) Lewis, B. P.; Shih, I. h.; Jones-Rhoades, M. W.; Bartel, D. P.; Burge, C. B. *Cell* **2003**, *115*, 787−798.
(39) Xia, Y.; Adibnia, V.; Huang, R.; Murschel, F.; Faivre, J.; Xie, G.; Olszewski, M.; De Crescenzo, G.; Qi, W.; He, Z.; Su, R.; Matyjaszewski, K.; Banquy, X. *Angew. Chem.* **2019**, *131*, 1322−1328.
(40) Molino, P. J.; Yang, D.; Penna, M.; Miyazawa, K.; Knowles, B. R.; MacLaughlin, S.; Fukuma, T.; Yarovsky, I.; Higgins, M. J. *ACS Nano* **2018**, *12*, 11610−11624.
(41) Xu, S.; Wu, Y.; Sun, X.; Wang, Z.; Luo, X. *J. Mater. Chem. B* **2017**, *5*, 4207−4213.
(42) Mei, Y.; Yu, K.; Lo, J. C. Y.; Takeuchi, L. E.; Hadjesfandiari, N.; Yazdani-Ahmadabadi, H.; Brooks, D. E.; Lange, D.; Kizhakkedathu, J. N. *ACS Nano* **2018**, *12*, 11881−11891.
(43) Soto, R. J.; Hall, J. R.; Brown, M. D.; Taylor, J. B.; Schoenfisch, M. H. *Anal. Chem.* **2017**, *89*, 276−299.
(44) Sun, Q.; Yan, F.; Yao, L.; Su, B. *Anal. Chem.* **2016**, *88*, 8364−8368.
(45) Feng, Q. M.; Shen, Y. Z.; Li, M. X.; Zhang, Z. L.; Zhao, W.; Xu, J. J.; Chen, H. Y. *Anal. Chem.* **2016**, *88*, 937−944.
(46) Ma, D.; Huang, C.; Zheng, J.; Tang, J.; Li, J.; Yang, J.; Yang, R. *Biosens. Bioelectron.* **2018**, *101*, 167−173.
(47) Xu, S.; Nie, Y.; Jiang, L.; Wang, J.; Xu, G.; Wang, W.; Luo, X. *Anal. Chem.* **2018**, *90*, 4039−4045.
(48) Xia, Y.; Wang, L.; Li, J.; Chen, X.; Lan, J.; Yan, A.; Lei, Y.; Yang, S.; Yang, H.; Chen, J. *Anal. Chem.* **2018**, *90*, 8969−8976.
(49) Yi, J.-T.; Chen, T.-T.; Huo, J.; Chu, X. *Anal. Chem.* **2017**, *89*, 12351−12359.
(50) Chang, J.; Wang, X.; Wang, J.; Li, H.; Li, F. *Anal. Chem.* **2019**, *91*, 3604−3610.
(51) Chen, X.; Liu, Y.; Xu, L.; Wang, Y.; Li, R.; Sun, P.; Lin, Z.; Yang, H. *Anal. Chem.* **2019**, *91*, 13712−13719.
(52) Liu, W.; Chen, A.; Li, S.; Peng, K.; Chai, Y.; Yuan, R. *Anal. Chem.* **2019**, *91*, 1516−1523.

https://dx.doi.org/10.1021/acs.analchem.0c00738
Anal. Chem. 2020, 92, 7186−7193